Feedback Linearization Based Nonlinear Control of SynRM Drives Accounting for Self- and Cross-Saturation

Angelo Accetta, *Member, IEEE*, Maurizio Cirrincione, *Senior Member, IEEE*, Marcello Pucci, *Senior Member, IEEE*, and Antonino Sferlazza, *Member, IEEE*

***Abstract*—This article proposes a nonlinear controller based on feedback linearization (FL) for synchronous reluctance motor (SynRM) drives which takes into consideration the magnetic saturation. The proposed nonlinear FL control based control technique has been developed starting from the theoretical definition of an original dynamic model of the SynRM taking into consideration both the self- and the cross-saturation effects. Such a control technique permits the dynamics of both the speed and axis flux loops to be maintained constant independently from the load and the saturation of the iron core in both constant flux and variable direct axis flux operating conditions. Finally, sensitivity of the performance of the proposed FL control versus the variation of the main motor parameters has been verified. The proposed technique has been tested experimentally on a suitably developed test setup. The proposed FL control has been further compared with the classic field-oriented control (FOC) in both constant flux and variable flux working conditions.**

***Index Terms*—Feedback linearization (FL), magnetic saturation, synchronous reluctance motors (SynRM).**

I. Introduction

SYNCHRONOUS reluctance motors (SynRMs) have been prototyped around 1923. Their low performance (in terms of output torque and power) combined with their relatively high price have, however, limited their adoption for a long time. Only recently, novel techniques for the advanced design of rotors have permitted increased values of the saliency ratios (9–12), to which the performance of SynRMs is strictly related [2]. Nowadays, even if modern SynRMs offer output power levels comparable to those of the corresponding induction motors (IMs), very limited number of industries produce them. One of the reasons is that due to their constructional characteristics, SynRMs can be hardly operated in open loop. High dynamic performance can be achieved by adopting vector control technique; indeed, several rotor-oriented control (ROC) or stator flux-oriented control (FOC) schemes have been developed [3]–[5]. The theoretical performance of the SynRMs is limited, however, by the strong nonlinearity of the machine, particularly because of its magnetic characteristics; actually, the saturation phenomena are different on the direct and quadrature axes, and significant cross-saturation phenomena are observable [6].

During the last years, several approaches for high-performance control of SynRM drives have been developed. In detail, [7] proposed unified direct-flux vector control scheme adopting a direct stator flux control approach implemented in the stator flux reference frame. The stator flux is directly controlled by the d-axis component of the stator voltage vector, while the torque is controlled by regulating the q-axis component of the stator current vector. The scope of [7] is more to device a general control scheme to be possibly used for all kinds of motors than to propose a high-performance control technique specifically conceived for SynRM drives. In [7], it is explicitly written that a coupling of the quadrature axis current equation with the direct axis exists during flux regulation transients only, which is typical of classic vector controllers. This is a concrete control problem of SynRM drives, given that they are typically operated under maximum torque per ampere (MTPA) operation. The control system theory offers an important set of nonlinear control methodologies for dealing with the nonlinearities of electric motors and tries to overcome exactly the above-mentioned limits of classic vector controllers.

Among nonlinear control techniques, one of the most promising is the so-called input–output feedback linearization (FL) [8], [9]. This issue has been faced up initially with specific regard to IM drives [10]–[12]. Nevertheless, very few applications of FL to SynRMs are still present in the scientific literature [13]–[16]. In particular, [13] proposes an adaptive input–output FL technique used for speed and torque-tracking control of a SynRM drive, assuming as state variables the direct and quadrature stator flux components and the rotor speed. This controller is capable of estimating online the motor static inductances on the two

Manuscript received July 7, 2021; revised November 22, 2021 and January 31, 2022; accepted February 22, 2022. Date of publication March 1, 2022; date of current version May 20, 2022. Paper 2021-IDC-0721.R2, presented at the 2019 IEEE Energy Conversion Congress and Exposition, Baltimore, MD USA, Sep. 29–Oct. 3, and approved for publication in the IEEE TRANSACTIONS ON INDUSTRY APPLICATIONS by the Industrial Drives Committee of the IEEE Industry Applications Society. This work was supported in part by the USP-SRT Research Project: Advanced Control of Synchronous Reluctance Motors for Electrical Vehicles (ACOSREV). *(Corresponding author: Marcello Pucci.)*

Angelo Accetta and Marcello Pucci are with the Institute for Marine Engineering (INM), National Research Council of Italy (CNR), 90146 Palermo, Italy (e-mail: angelo.accetta@cnr.it; marcello.pucci@cnr.it).

Maurizio Cirrincione is with the School of Engineering and Physics, University of the South Pacific, Laucala Campus, Suva 0679, Fiji (e-mail: cirrincione_m@usp.ac.fj).

Antonino Sferlazza is with the Department of Energy, Information Engineering, and Mathematical Models, University of Palermo, 90128 Palermo, Italy (e-mail: antonino.sferlazza@unipa.it).

Color versions of one or more figures in this article are available at https://doi.org/10.1109/TIA.2022.3155511.

Digital Object Identifier 10.1109/TIA.2022.3155511

0093-9994 © 2022 IEEE. Personal use is permitted, but republication/redistribution requires IEEE permission.
See https://www.ieee.org/publications/rights/index.html for more information.

Authorized licensed use limited to: University of the South Pacific. Downloaded on June 08,2022 at 06:52:22 UTC from IEEE Xplore. Restrictions apply.

axes. The work [14] proposed an FL control technique whose main control objective is the minimization of SynRM power losses under the constraint of constant torque production. To this aim, [14] includes the iron losses in the SynRM model, but it neglects the iron saturation phenomenon. In [15], a nonlinear controller is proposed, which directly regulates the torque by selecting the product of d- and q-axis currents, concurring to the production of the torque as one of the output variables. In [16], an approach similar to the two previous papers is followed, but only the rotor speed has been estimated. Finally, [17] proposes an input–output FL technique, permitting the decoupling of the stator flux and electromagnetic torque control loops. In [17], the controller equations are based on the SynRM dynamic model expressed in the stator flux reference frame. The dynamic model exploited in [17], however, does not take into account the magnetic saturation.

The input–output feedback linearization control (FLC) technique is, however, a model-based control and, therefore, suffers primarily from two disadvantages: 1) the accuracy of the dynamic model on which the control law is based; and 2) the corresponding correct knowledge of the model parameters. Starting from these remarks, this article, differently from the previous papers presented in literature, proposes a nonlinear controller based on input–output FLC for SynRM drives based on an original accurate dynamic model taking into consideration the self- and cross-saturation effects. The proposed FLC technique considering the magnetic saturation has been verified experimentally on a suitably developed test setup. It has been experimentally compared with field-oriented control (FOC), in particular with the ROC. Experimental tests have been performed in both constant flux and variable flux working conditions. As for the variable flux operation, the SynRM drive has been integrated with the MTPA technique proposed in [18]. Finally, a sensitivity analysis has been made, showing the effects on the performance of the proposed FLC of a strong detuning of the main motor parameters (inductances and resistances).

A. Comparison With the Scientific Literature

The proposed FLC assumes as state variables the direct and quadrature components of the stator currents and the rotor speed. The space-vector dynamic model on the basis of which the proposed FLC has been developed is inspired from [19], whose magnetic model has been proposed in [20], improving it in a far better mathematical description of the cross-saturation phenomenon. As for the control law, the proposed FLC follows the approach in [10] and [11], where the chosen state variable on the quadrature axis is rotor speed and not the electromagnetic torque. From this point of view, this work differs from [14] and [17], where only the stator equations have been linearized by state feedback. In the proposed approach, speed control is performed so that the dynamics of the torque are controlled as internal dynamics of the system but without the need of a dedicated control loop, as it is the case of FOC and FLC in [17] in which the controlled variables are torque and flux. The approach in [17], therefore, requires the adoption of two controllers on the quadrature axis (torque and speed), whereas the proposed approach requires only one (speed). To follow the proposed approach, the mechanical dynamics of the system, and, therefore, the inertia of the motor, must be accounted for, to define the suitable set of nonlinear transformations of the states and inputs. As for the FLC proposed in [13], since it assumes the stator flux components as state variables besides the speed, it reveals necessarily simpler than the proposed one, regarding the dynamic model. Moreover, it presents the advantage of being adaptive with the variation of the direct and quadrature static inductances. This advantage is, however, paid by the fact that the control system requires online knowledge of the stator flux direct and quadrature components. These quantities cannot be measured online while they are to be estimated by flux models or observers. The control system performance and the accuracy in the estimation of the inductances in [13], thus, suffer also from the accuracy of the stator flux components by the flux model. On the contrary, the proposed FLC requires the online knowledge of the stator current components, which are measured quantities, and, thus, it is intrinsically more accurate than [13] and potentially more performing. Finally, all the works in literature dealing with the FLC of SynRMs do not consider the self- and cross-saturation effects to the best of the authors' knowledge, and this is one of the major contributions of this work.

II. Space-Vector State Model of the SynRM Considering Self- and Cross-Saturation

A complete magnetic model of the SynRM has been proposed in [20], where specific original flux versus current functions have been deduced, permitting both the self- and cross-saturation effects to be accounted for. Correspondingly, [19] proposed a new space-vector model of the SynRM including self- and cross-saturation effects expressed in state form. The definition of such a model is crucial for developing the nonlinear FL technique proposed in this article. The magnetic model proposed in [19] has been significantly improved here in order to better describe the cross-saturation phenomenon.

A. Literature Review of Magnetic Models of SynRMs

The work [21] presents a review of some explicit functions for modeling the magnetic saturation of SynRM, dividing them into two major approaches: 1) the flux versus current, to be used when the current is assumed as a state variable; 2) the current versus flux ones, to be used when the flux is assumed as the state variable. As for the current versus flux approach, two kinds of functions are cited: 1) the power function [22]; 2) the arctan function (modeling the derivative of the current to the flux and thus to be integrated) [23]. None of them, however, accounts for the cross-saturation phenomenon. As for the flux versus current approach, three kinds of functions are cited: 1) piecewise functions proposed in [24] for describing only the self-saturation and improved in [25] by integrating the cross-saturation; 2) the polynomial functions [26] accounting for the cross-saturation; 3) the rational functions [27] accounting for the cross-saturation but not fulfilling the reciprocity conditions. In particular, [21] proposes a magnetic model belonging to the current versus flux approach and based on an improved version

Authorized licensed use limited to: University of the South Pacific. Downloaded on June 08,2022 at 06:52:22 UTC from IEEE Xplore. Restrictions apply.

of the power function accounting also for the cross-saturation and respecting the reciprocity condition. In [28], the authors address the issue of the experimental magnetic characterization of the flux versus current relationship of interior permanent magnet (IPMs) and permanent magnet (PM)-assisted SynRMs. In particular, a simplified but effective model of the cross-saturation phenomenon is proposed.

B. Proposed Magnetic Model

The proposed magnetic model is in the framework of a flux versus current approach; so it is suitable for dynamic models of SynRMs adopting the stator currents as state variables. As for the magnetic characteristics of the SynRM, the following functions are proposed, which consider both the self- and cross-saturation effects and describe the relationships between the direct and quadrature components of the stator fluxes and the corresponding components of the stator currents in the synchronous reference frame. The stator flux direct (x) and quadrature (y) components have been defined as follows:

$$\psi_{sx} = 2\alpha_1\left(\frac{1}{1+\mathrm{e}^{-\beta_1 i_{sx}}} - \frac{1}{2}\right) + \eta_1 i_{sx} + \Delta\psi_{sx} \tag{1a}$$

$$\psi_{sy} = 2\alpha_2\left(\frac{1}{1+\mathrm{e}^{-\beta_2 i_{sy}}} - \frac{1}{2}\right) + \eta_2 i_{sy} + \Delta\psi_{sy}. \tag{1b}$$

Tb. I show the complete list of the adopted symbols. In particular, as for the self-saturation, it has been formulated by adopting sigmoid functions, to which linear functions are added because the magnetic characteristic of the motor is not completely flat in deep saturation. As for the cross-saturation, it has been conceived starting from the definition of a proper coenergy variation function due to the cross-saturation. The coenergy variation function has been expressed as the product of two functions, one depending only on i_{sx} and the other depending only on i_{sy}. This last condition is very important since it permits the reciprocity conditions to be properly fulfilled. The mathematical formulation has been created based on the analysis of [29, Fig. 2]. This last figure shows that the flux on the x-axis reduces for increasing values of the current i_{sy}. Moreover, for a given value of i_{sx}, the amount of reduction of the flux on the x-axis depends on the absolute value of i_{sy}, being independent from its sign. The higher the absolute value of i_{sy} is, the higher the flux reduction on the x-axis is. Moreover, the same figure shows that the flux variation on the x-axis is null for zero value of i_{sx} and very little for high values of i_{sx}, while it presents a maximum for a certain intermediate range of i_{sx}. These considerations suggest that the flux variation on the x-axis should be weighted with a function of i_{sx} presenting a bell shape. Since it is needed that such a function presents a primitive (for the definition of the coenergy variation function), the derivative of the sigmoid function has been chosen, which is a combination of exponentials. In particular, the defined coenergy variation function is the following:

$$\Delta W' = \gamma \frac{1}{\left(1+\mathrm{e}^{\frac{-(i_{sx}-\mu_1\mathrm{sgn}(i_{sx}))\mathrm{sgn}(i_{sx})}{\sigma_1}}\right)} \frac{1}{\left(1+\mathrm{e}^{\frac{-(i_{sy}-\mu_2\mathrm{sgn}(i_{sy}))\mathrm{sgn}(i_{sy})}{\sigma_2}}\right)}. \tag{2}$$

From (2), the cross-saturation flux variation terms can be computed as

$$\Delta\psi_{sx} = \frac{d\Delta W'}{di_{sx}} = -l_{xx}l_{xy}, \tag{3a}$$

$$\Delta\psi_{sy} = \frac{d\Delta W'}{di_{sy}} = -l_{yy}l_{yx} \tag{3b}$$

where l_{xx}, l_{xy}, l_{yy}, and l_{yx} are given in the Appendix.

Since the nonlinear inductor should not generate or dissipate electrical energy, the reciprocity condition must be satisfied [21], [30], and the cross-saturation dynamic inductance can be coherently defined as

$$L'_{sxy} = \frac{d\Delta\psi_{sx}}{di_{sy}} = \frac{d\Delta\psi_{sy}}{di_{sx}} = -\frac{1}{\gamma} l_{xx} l_{yy}. \tag{4}$$

The analysis of (4) shows that, independently from the numerical values of the parameters, the sign requirements described in [31] are satisfied. Finally, the self-saturation dynamic inductances on the direct and quadrature axes can be defined as

$$L'_{sxx} = \frac{d\psi_{sx}}{di_{sx}} = \\ = \eta_1 + \frac{2\alpha_1\beta_1}{\left(\mathrm{e}^{\frac{\beta_1 i_{sx}}{2}} + \mathrm{e}^{-\frac{\beta_1 i_{sx}}{2}}\right)^2} + \frac{1}{\sigma_1}\mathrm{sgn}(i_{sx}) l_{xx} l_{xy} l'_x, \tag{5a}$$

$$L'_{syy} = \frac{d\psi_{sy}}{di_{sy}} = \\ = \eta_2 + \frac{2\alpha_2\beta_2}{\left(\mathrm{e}^{\frac{\beta_2 i_{sy}}{2}} + \mathrm{e}^{-\frac{\beta_2 i_{sy}}{2}}\right)^2} + \frac{1}{\sigma_2}\mathrm{sgn}(i_{sy}) l_{yy} l_{yx} l'_y \tag{5b}$$

where l'_x and l'_y are given in the Appendix.

As for the static inductances, they are straightforwardly defined as

$$L_{sxx} = \frac{\psi_{sx}}{i_{sx}} = \eta_1 + 2\alpha_1\left(\frac{1}{1+\mathrm{e}^{-\beta_1 i_{sx}}} - \frac{1}{2}\right)\frac{1}{i_{sx}} - \frac{l_{xx}l_{xy}}{i_{sx}}, \tag{6a}$$

$$L_{syy} = \frac{\psi_{sy}}{i_{sy}} = \eta_2 + 2\alpha_2\left(\frac{1}{1+\mathrm{e}^{-\beta_2 i_{sy}}} - \frac{1}{2}\right)\frac{1}{i_{sy}} - \frac{l_{yy}l_{yx}}{i_{sy}}. \tag{6b}$$

The entire magnetic behavior of the machine can be, therefore, described by functions requiring the knowledge of 11 model parameters (α_1, β_1, η_1, γ, μ_1, σ_1, α_2, β_2, η_2, μ_2, and σ_2), of which 6 describe the self-saturation on both axes (α_1, β_1, η_1, α_2, β_2, and η_2) and 5 describe the cross-saturation (γ, μ_1, σ_1, μ_2, and σ_2). The parameters of the proposed have been identified by adopting the methodology presented in [32].

As for the SynRM under test, whose photo is shown in Fig. 9 and rated values and model's parameters are described in Tables IV and V, Fig. 1 shows the variation of the static self-inductance on the direct (quadrature) axis versus the direct (quadrature) axis current for several values of the quadrature (direct) current, defined in (6). These figures show a set of curves, obtained respectively for zero current on the other axis (no cross-saturation is present) as well as for increasing values of the current on the other axis. It can be observed that L_{sxx} decreases with i_{sx}, as expected because of the self-saturation

Authorized licensed use limited to: University of the South Pacific. Downloaded on June 08,2022 at 06:52:22 UTC from IEEE Xplore. Restrictions apply.

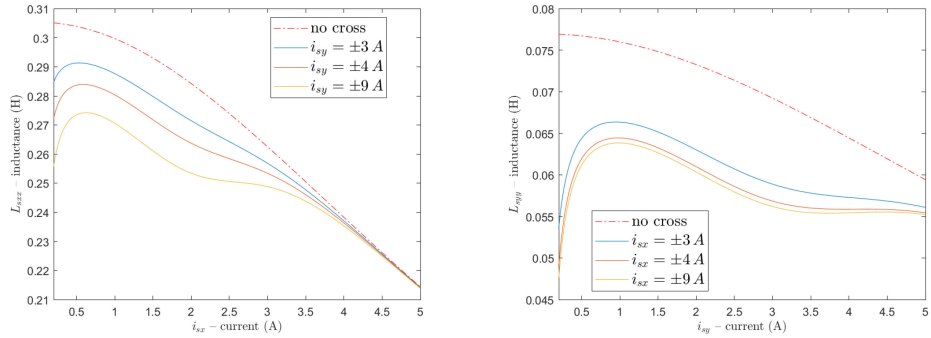

Fig. 1. Static self-inductance on the direct axis L_{sxx} and on the quadrature axis L_{syy} for several values of the current.

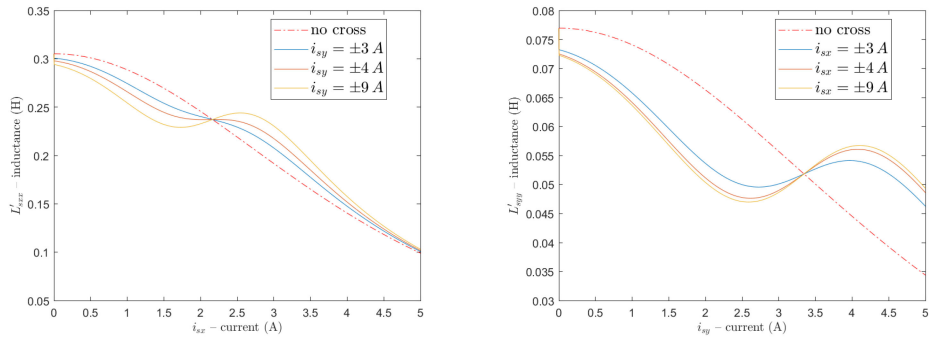

Fig. 2. Dynamic self-inductance on the direct axis L'_{sxx} and on the quadrature axis L'_{syy} for several values of the current.

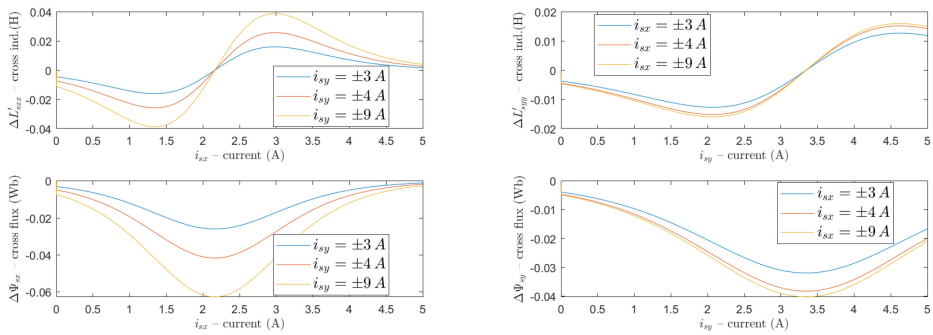

Fig. 3. Cross-saturation terms of the dynamic self-inductance on the direct and quadrature axes for several values of the current (top plots) and cross-saturation flux (bottom plots).

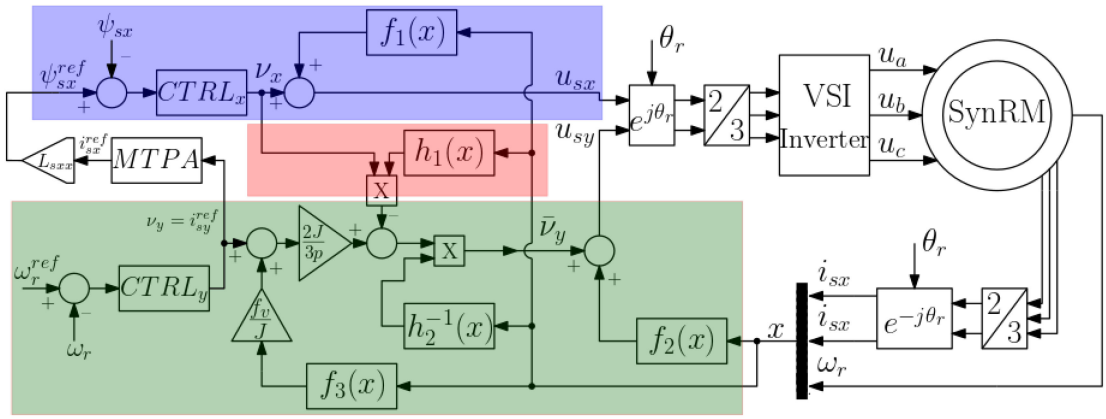

Fig. 4. Block diagram of the proposed controller.

Authorized licensed use limited to: University of the South Pacific. Downloaded on June 08,2022 at 06:52:22 UTC from IEEE Xplore. Restrictions apply.

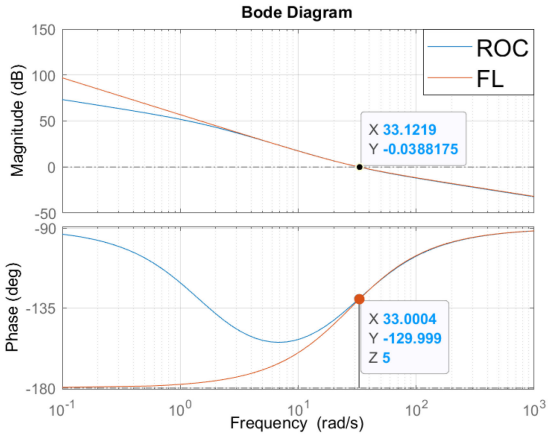

Fig. 5. Bode diagram: open-loop transfer function for direct axis flux dynamics.

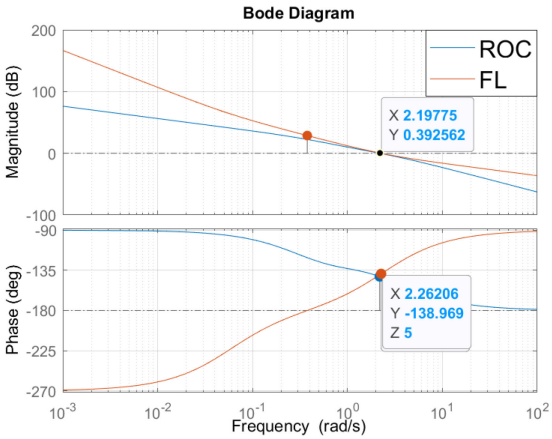

Fig. 6. Bode diagram: open-loop transfer function for speed dynamics.

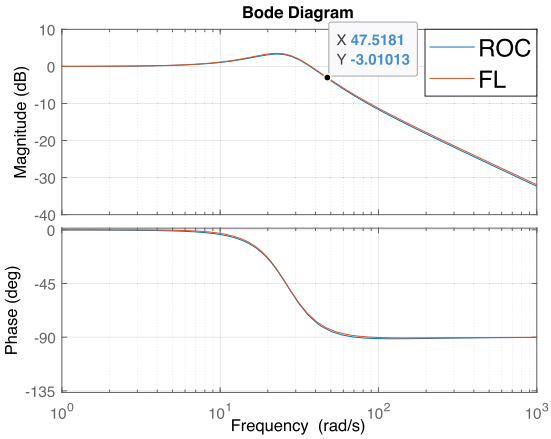

Fig. 7. Bode diagram: closed-loop transfer functions of the direct axis flux dynamics.

phenomenon. It can be further observed that L_{sxx} decreases for increasing values of i_{sy}. The higher the i_{sy} is, the lower is the L_{sxx}; in particular, the inductance curves obtained with nonnull values of i_{sy} are lower than that obtained with the null value of i_{sy} for any value of i_{sx}. The same phenomenon is observable on L_{syy}. As for the dynamic self-inductance defined in (5),

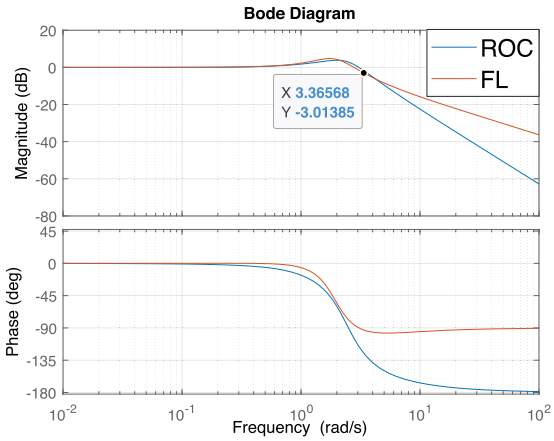

Fig. 8. Bode diagram: closed-loop transfer functions of the speed dynamics.

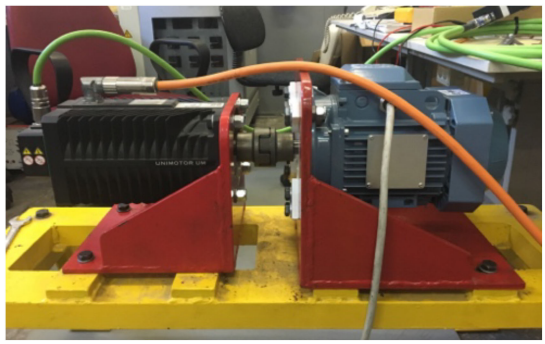

Fig. 9. Photograph of the SynRM experimental setup.

TABLE I
LIST OF SYMBOLS

u_{sx}, u_{sy}	stator voltages in the rotor oriented reference frame;
i_{sx}, i_{sy}	stator currents in the rotor oriented reference frame;
ψ_{sx}, ψ_{sy}	stator fluxes in the rotor oriented reference frame;
L_{sxx}, L_{syy}	self static inductances along x and y axes;
L_{sxy}, L_{syx}	cross static inductances;
L'_{sxx}, L'_{syy}	self dynamic inductances along x and y axes;
L'_{sxy}, L'_{syx}	cross dynamic inductances;
R_s	stator resistance;
ω_r	angular speed of the rotor (mechanical angles);
t_m	electromagnetic torque generated by the motor;
t_l	load torque;
p	pole-pairs;
J	rotor inertia;
f_v	viscous friction coefficient.

TABLE II
PARAMETERS OF THE CONTROLLERS

ROC		*FL*	
Direct flux-loop	Speed-loop	Direct flux-loop	Speed-loop
$k_{p,\psi} = 24.2$	$k_{p,\omega} = 0.15$	$k_{p,\psi} = 25.3$	$k_{p,\omega} = 3.86$
$k_{i,\psi} = 723$	$k_{i,\omega} = 0.30$	$k_{i,\psi} = 700$	$k_{i,\omega} = 0.22$
			$k_{d,\omega} = 1.53$

TABLE III
DESIGN SPECIFICS

	SPEED	DIRECT FLUX
Crossing pulsation	$\bar{\omega}_t = 2.2$ rad/s	$\bar{\omega}_t = 33$ rad/s
Phase margin	$m_\phi = 38°$	$m_\phi = 50°$

Authorized licensed use limited to: University of the South Pacific. Downloaded on June 08,2022 at 06:52:22 UTC from IEEE Xplore. Restrictions apply.

TABLE IV
RATED DATA OF THE SYNRM

SYMBOLS	VALUES
Rated power (kW)	2.2
Rated voltage (V)	380
Rated frequency (Hz)	50
Pole-pairs	2
Rated speed (rpm)	1500
Rated current (A)	5.5
Rated torque (Nm)	14

TABLE V
PARAMETERS OF THE SYNRM SATURATION MODEL

SYMBOL	VALUE	SYMBOL	VALUE
α_1	1.2139	γ	0.156
β_1	0.4848	μ_1	2.161
η_1	0.0111	σ_1	0.622
α_2	0.3609	μ_2	3.343
β_2	0.4033	σ_2	0.971
η_2	0.0042	R_0	8142

Fig. 2 shows the variation of the dynamic self-inductance on the direct (quadrature) axis versus the direct (quadrature) axis current for several values of the quadrature (direct) current. The shapes of dynamic inductances are similar to those of the static ones, with some differences highlighted in the following. It can be observed that the direct axis dynamic self-inductance curve obtained for nonnull values of quadrature axis current, below a certain current threshold and for increasing values of the direct axis current, is lower than that obtained for zero quadrature axis current (no cross-saturation). The reason is the reduction of the direct axis flux caused by the further saturation of the self-axis by the quadrature current. The shape of the dynamic self-inductance above this threshold of direct axis current changes. In fact, the direct axis flux reduction caused by the cross-saturation is not equal in the entire range of the direct axis current. It is null for zero direct axis current, then it increases getting a maximum, and then it starts decreasing to a limited value because the magnetic circuit is already fully saturated by the direct axis current. On the quadrature axis, the self-flux reduction due to the direct axis current, above a certain value of quadrature current, is less observable. This phenomenon is coherent with the fact that the quadrature axis magnetic circuit gets less easier the full saturation. The above-described kind of variation is confirmed also in [29, Fig. 2]. As for the proposed magnetic model, such a phenomenon is shown in Fig. 3 (bottom plots), showing the flux reduction on both axes caused by the cross-saturation. Since the dynamic direct axis self-inductance is defined as the derivative of the direct axis flux with respect to the direct axis current, the component of the direct axis dynamic self-inductance due to the cross-saturation changes its sign above a certain value of direct axis current (see Fig. 3, top plots). This phenomenon finally motivates why a certain value of direct axis current exists, above which the direct axis dynamic self-inductance obtained with a nonnull value of the quadrature axis current becomes higher than that obtained for zero quadrature axis.

The proposed FLC control technique assumes an *a priori* knowledge of the magnetic behavior of the SynRM. This is a slight complication of the control law; all the inductance functions have to be implemented online, and, thus, the related parameters must be previously identified offline. In the authors' opinion, however, this does not limit the application of the proposed method to other machines with different ratings. As a matter of fact, the methodology for identifying offline the model parameters defined in [20] is based on three simple stand-still tests that do not require the machine to be run at any speed or load. The tests just require the SynRM to be supplied by a voltage source inverter (VSI) that is something implicit in its adoption. The offline identification procedure can be easily integrated in the control action as a preliminary self-commissioning phase, within which even the controller tuning can be included. In general, a proper tuning of the current regulators of a SynRM drive would require, in any case, a proper magnetic characterization of the machine.

The static and dynamic inductance surfaces function, if straightforwardly implemented, would require a very high computational demand. In this case, however, all these surfaces have been experimentally implemented as linearly interpolated functions, thus reducing significantly the computational demand.

C. Dynamic Model of the SynRM

If $\mathbf{\Psi}_s = [\psi_{sx},\ \psi_{sy}]$ is the vector whose elements are the direct and quadrature stator flux components in the rotor reference frame and $\mathbf{i}_s = [i_{sx},\ i_{sy}]$ is the corresponding stator current components vector, the complete space-vector dynamic model of the SynRM in state form, selecting the stator fluxes as state variables, can be written as

$$\frac{d\mathbf{\Psi}_s}{dt} = \mathbf{u}_s - R_s\mathbf{i}_s - j\omega_r\mathbf{\Psi}_s. \tag{7}$$

The stator current can be obtained from the stator fluxes by means of the following relations:

$$i_{sx} = L_{sxx}^{-1}\psi_{sx}, \quad i_{sy} = L_{syy}^{-1}\psi_{sy} \tag{8}$$

where the expressions of L_{sxx} and L_{sxx} are given in (6).

By replacing (6) with (8) and properly differentiating, model (7) can be also conveniently written by considering the stator currents as state variables, instead of the stator fluxes, as follows:

$$\frac{d\mathbf{i}_s}{dt} = \mathbf{L}_s'^{-1}\left(\mathbf{u}_s - R_s\mathbf{i}_s - jp\omega_r\mathbf{\Psi}_s\right). \tag{9}$$

The inverse matrix of the dynamic inductances in (9) is defined as

$$\mathbf{L}_s'^{-1} = \frac{1}{L'_{sxx}L'_{syy} - L'^{2}_{sxy}}\begin{bmatrix} L'_{sxx} & -L'_{sxy} \\ -L'_{sxy} & L'_{syy} \end{bmatrix} \tag{10}$$

where L'_{sxx}, L'_{syy}, and L'_{sxy} and their expressions are given in (4) and (5).

Finally, the mechanical equation of the SynRM is given by

$$J\frac{d\omega_r}{dt} = -f_v\omega_r + t_m - t_l \tag{11}$$

where J and f_v are the moment of inertia and the viscous friction coefficient, t_l is the load torque, and t_m is the electromagnetic

Authorized licensed use limited to: University of the South Pacific. Downloaded on June 08,2022 at 06:52:22 UTC from IEEE Xplore. Restrictions apply.

torque produced by the motor and is given by

$$t_m = \frac{3}{2}p\left(\psi_{sx}i_{sy} - \psi_{sy}i_{sx}\right) = \frac{3}{2}p\left(L_{sxx} - L_{syy}\right)i_{sx}i_{sy} = \frac{3}{2}p\left(\frac{1}{L_{syy}} - \frac{1}{L_{sxx}}\right)\psi_{sx}\psi_{sy}. \tag{12}$$

It is noteworthy that only the expression of the static inductances appears in the dynamics of the speed since the electromagnetic torque is explicitly dependent on the static inductances, and it depends on the dynamic inductances only indirectly through the stator fluxes.

III. Nonlinear Controller Design

Let us suppose that the SynRM drive is operated under ROC or FOC or any FLC not involving the speed loop in the controller design. If the controlled variables are the direct axis current (proportional to the direct axis flux by the direct static self-inductance) and the rotor speed, assuming that the drive is operated under MTPA (variable direct axis current), the speed and the direct axis control loops are coupled by the torque expression (12). The only way to decouple the speed and direct axis current loops is to adopt a suitably defined FLC accounting for the mechanical dynamic equation. In the following, the proposed approach is described. To design the controller, (7), (9), and (11) are now considered. Moreover, the two outputs of this model are represented by the direct axis flux ψ_{sx} and the mechanical speed ω_r. Note that this system is a multiple-input multiple-output system; therefore, a state feedback will be designed so that the resulting system can be viewed as two decoupled systems: The first governs the ψ_{sx} dynamics and the second governs the ω_r dynamics. Finally, the target of the proposed controller is the full decoupling between these two systems in any operating condition, independently of the load and the saturation condition.

With regard to the direct axis flux dynamics, if the Lie derivative of ψ_{sx} is computed, the first equation of (7) is obtained. This means that if the state vector is defined as

$$x := \begin{bmatrix} i_{sx} & i_{sy} & \omega_r \end{bmatrix}^\top \tag{13}$$

and the input u_{sx} is designed such that

$$u_{sx} = R_s i_{sx} - \omega_r \psi_{sy} + \nu_x := f_1(x) + \nu_x, \tag{14}$$

then the dynamics of ψ_{sx} can be written in terms of the new input ν_x as follows:

$$\frac{d\psi_{sx}}{dt} = \nu_x. \tag{15}$$

With regard to the speed dynamics, if the new state variable a, called *acceleration* and defined as $a := \frac{d\omega}{dt}$, is introduced, then it is possible to compute the second-order Lie derivative of the speed along the trajectories of the system as follows:

$$\frac{d\omega^2}{dt^2} = -\frac{f_v}{J}a + \frac{3p}{2J}\left(\begin{bmatrix} g_1 & g_2 \end{bmatrix}\mathbf{L}_s'^{-1} + \left(\frac{1}{L_{syy}} - \frac{1}{L_{sxx}}\right)\begin{bmatrix}\psi_{sy} & \psi_{sx}\end{bmatrix}\right)\begin{bmatrix} u_{sx} - R_s i_{sx} + \omega_r\psi_{sy} \\ u_{sy} - R_s i_{sy} - \omega_r\psi_{sx}\end{bmatrix} \tag{16}$$

where

$$g_1 := \left(\frac{\frac{\partial L_{sxx}}{\partial i_{sx}}}{L_{sxx}^2} - \frac{\frac{\partial L_{syy}}{\partial i_{sx}}}{L_{syy}^2}\right) = \frac{1}{i_{sx}}\left(\frac{L'_{sxx} - L_{sxx}}{L_{sxx}^2}\right) + \frac{1}{i_{sy}}\left(\frac{L'_{syx}}{L_{syy}^2}\right), \tag{17a}$$

$$g_2 := \left(\frac{\frac{\partial L_{sxx}}{\partial i_{sy}}}{L_{sxx}^2} - \frac{\frac{\partial L_{syy}}{\partial i_{sy}}}{L_{syy}^2}\right) = \frac{1}{i_{sy}}\left(\frac{L'_{syy} - L_{syy}}{L_{syy}^2}\right) + \frac{1}{i_{sx}}\left(\frac{L'_{sxy}}{L_{sxx}^2}\right). \tag{17b}$$

As can be seen from (16), both the inputs u_{sx} and u_{sy} appear in the expression. Then the model in this form cannot be feedback linearizable in the "classical" form since the dynamic of speed cannot be made independent of the control of ψ_{sx}. However, from (14) and (15), it is apparent that the dynamics of ψ_{sx} do not depend on u_{sy}. This suggests considering the two systems as a cascade of two subsystems: the first that describes the ψ_{sx} dynamics and the second that describes the ω_r dynamics. In this way, it is possible to design ν_x [and, consequently, u_{sx} by (14)] in order to assign the dynamics of (15) and then to consider ν_x as a time-varying quantity that perturbs the second subsystem (the one of the speed). Obviously, ν_x is known and it will be necessary to compute the feedback law to linearize the speed dynamics. In other words, the following is defined:

$$u_{sy} = R_s i_{sy} + \omega_r \psi_{sx} + \bar{\nu}_y := f_2(x) + \bar{\nu}_y \tag{18}$$

and by considering (14), (16) can be written as

$$\frac{d\omega^2}{dt^2} = -\frac{f_v}{J}a + \frac{3p}{2J}\left(h_1(x)\nu_x + h_2(x)\bar{\nu}_y\right) \tag{19}$$

where

$$h_1(x) := \frac{g_1 L'_{sxx} + g_2 L'_{sxy}}{L'_{sxx}L'_{syy} - L'^2_{sxy}} + \left(\frac{1}{L_{syy}} - \frac{1}{L_{sxx}}\right)\psi_{sy}, \tag{20a}$$

$$h_2(x) := \frac{g_1 L'_{sxy} + g_2 L'_{syy}}{L'_{sxx}L'_{syy} - L'^2_{sxy}} + \left(\frac{1}{L_{syy}} - \frac{1}{L_{sxx}}\right)\psi_{sx}. \tag{20b}$$

At this point, it is possible to define the auxiliary input $\bar{\nu}_y$ as

$$\bar{\nu}_y := h_2^{-1}(x)\left(-h_1(x)\nu_x + \frac{2J}{3p}\left(\frac{f_v}{J}a + \nu_y\right)\right) = h_2^{-1}(x)\left(-h_1(x)\nu_x + \frac{2J}{3p}\left(f_3(x) + \nu_y\right)\right) \tag{21}$$

with

$$f_3(x) := \frac{f_v}{J^2}\left(\frac{3}{2}p\left(\frac{1}{L_{syy}} - \frac{1}{L_{sxx}}\right)\psi_{sx}\psi_{sy} - f_v\omega_r - t_l\right) \tag{22}$$

Authorized licensed use limited to: University of the South Pacific. Downloaded on June 08,2022 at 06:52:22 UTC from IEEE Xplore. Restrictions apply.

where ν_y is a new auxiliary input. With the above definition, the system describing the speed dynamics becomes

$$\frac{d\omega_r}{dt} = a, \qquad \frac{da}{dt} = \nu_y \tag{23}$$

which appears in the standard linear form.

Note that each state function $f_1(x)$, $f_2(x)$, $f_3(x)$, $h_1(x)$, and $h_2(x)$, appearing in the scheme of Fig. 4, can be conveniently written as only functions of the currents i_{sx}, i_{sy}, and the speed ω_r, which are all measurable quantities. Indeed, by considering the above given relationships, it is possible to write

$$f_1(x) := R_s i_{sx} - \omega_r L_{syy} i_{sy}, \tag{24a}$$

$$f_2(x) := R_s i_{sy} + \omega_r L_{sxx} i_{sx}, \tag{24b}$$

$$f_3(x) := \frac{f_v}{J^2}\left(\frac{3}{2} p\left(L_{sxx} - L_{syy}\right) i_{sx} i_{sy} - f_v \omega_r - t_l\right), \tag{24c}$$

$$h_1(x) := \frac{g_1 L'_{sxx} + g_2 L'_{sxy}}{L'_{sxx} L'_{syy} - {L'_{sxy}}^2} + \left(1 - \frac{L_{syy}}{L_{sxx}}\right) i_{sy}, \tag{24d}$$

$$h_2(x) := \frac{g_1 L'_{sxy} + g_2 L'_{syy}}{L'_{sxx} L'_{syy} - {L'_{sxy}}^2} + \left(\frac{L_{sxx}}{L_{syy}} - 1\right) i_{sx} \tag{24e}$$

where g_1 and g_2, given in (17), as well as the static and dynamic inductances, given in (4)–(6), are already expressed as functions of the currents i_{sx} and i_{sy}.

Remark 1: The proposed control scheme requires the existence of the inverse of $h_2(x)$, $h_2^{-1}(x)$. However, it is possible to prove that the inverse exists if $\psi_{sx} \neq 0$, and this condition is always satisfied because the SynRM works properly only if the direct axis flux ψ_{sx} is strictly greater than zero for any working condition. Thus, the condition $\psi_{sx} > 0$ ensures that the mapping $h_2^{-1}(x) h_1(x)$ is a diffeomorphism, i.e., it is an invertible function that maps one differentiable manifold to another so that both the function and its inverse are smooth.

Remark 2: Note that the complication of considering the auxiliary input ν_x in the definition of the state feedback to linearize the speed dynamics has never been considered and tested in past works. This problem comes from the fact that self- and cross-saturation effects in the model imply the dependency of the inductances on the stator current.

The block diagram of the suggested control scheme is shown in Fig. 4, where the part related with direct axis flux control is highlighted with blue color, the part related with speed control is highlighted with green color, and how the auxiliary input ν_x enters for linearizing the speed dynamics is highlighted with red color.

A. Computation Requirement of the FL

As for the online computational effort, it is certainly higher with the proposed FLC than that required by the classic FOC. Both FL and FOC require the vector rotations from and to the synchronous reference frame. Both of them require a flux model (or observer) if closed-loop flux control is to be performed. The difference between the two lies primarily in the nonlinear transformations (14) and (18). As for the magnetic model that is embedded in the FL controller, all the analytical functions defining it, which are highly nonlinear and computationally demanding, once the model is identified offline, have been implemented online as linearly interpolated lookup tables, thus significantly reducing the overall computational effort. In particular, the turnaround time has been evaluated in both cases, which is strictly related to the execution time of the code. It is $8 \cdot 10^{-6}$ s for the FOC and 10^{-5} s for the proposed FL, which means that the required execution time is only 20% higher. This percentage can probably be further reduced by optimizing the control code. It is noteworthy that the measurement of the execution time or "turnaround time" as called in the DS1103 interface, is an actual measurement and not an estimation; it is the actual time that the board uses to complete a computational cycle of the application loaded onto the board itself.

B. Controller Design

In Fig. 4, the controller called CTRL$_x$ is a PI-type controller designed to assign a suitable closed-loop dynamics to system (15), while the controller called CTRL$_y$ is a PID-type controller designed to assign a suitable closed-loop dynamics to system (23). The two controllers are driven by the direct axis flux and rotor speed errors, respectively. Note that the two controllers can be designed independently of each other, so that the respective error dynamics can be asymptotically stable.

In particular, for direct axis flux dynamics, a PI controller has been adopted, whose transfer function is given by

$$G_{c,\psi} = k_{p,\psi} + \frac{k_{i,\psi}}{s}. \tag{25}$$

Although system (15) already contains a pole in $s = 0$, a PI controller (which introduces a further pole in $s = 0$ and a zero in $s = \frac{k_{i,\psi}}{k_{p,\psi}}$) is employed because system (15) is obtained only for a perfect parameters knowledge. As a consequence, if the integral action is not included in the controller, nonzero steady-state errors can occur. In this way, the system is more robust against parameter uncertainties. This is an important theoretical issue that has been been further demonstrated in the tests shown in Section V-C. For speed dynamics, a PID controller has been adopted, whose transfer function is given by

$$G_{c,\omega} = k_{p,\omega} + \frac{k_{i,\omega}}{s} + \frac{k_{d,\omega} s}{1 + \frac{k_{d,\omega}}{k_{p,\omega} N} s} \tag{26}$$

where $N > 10$. In this case, an integral action has been included for robustness reasons. However, since the speed dynamics are governed by a double integrator [see (23)], a derivative action is necessary to ensure stability of the closed-loop system and give a positive contribution to the phase to assign a suitable phase margin.

To verify the improvements in the dynamic performance achievable with the adoption of the proposed control technique, it will be compared with the industrial standard in high performance control of SynRM drives: the FOC. Among the different FOC algorithms, the ROC has been adopted here for comparison purposes. In detail, to compare the FLC to the ROC, the controller parameters $k_{p,\psi}$, $k_{i,\psi}$, $k_{p,\omega}$, $k_{i,\omega}$, and $k_{d,\omega}$ and the parameters of the PI in the ROC should be chosen so that the two

Authorized licensed use limited to: University of the South Pacific. Downloaded on June 08,2022 at 06:52:22 UTC from IEEE Xplore. Restrictions apply.

closed-loop systems present the same dynamics. In this case, the same crossing pulsation $\bar{\omega}_t$ and the same phase margin $\bar{m}_\phi$ are imposed, by designing the controller so that

$$|G_c(j\bar{\omega}_t)||G_p(j\bar{\omega}_t)| = 1, \tag{27a}$$

$$\arg(G_c(j\bar{\omega}_t)) + \arg(G_p(j\bar{\omega}_t)) + \pi = \bar{m}_\phi \tag{27b}$$

where $\bar{\omega}_t$ and $\bar{m}_\phi$ are the design crossing pulsation and phase margin, respectively, $G_c(\cdot)$ is either (25) or (26), and $G_p(\cdot)$ is either (15) or (23). It should be noted that, while in the proposed FLC the controlled variable is the direct axis flux, in ROC, the controlled variable is the direct axis current. To make the design of the control systems of FLC and ROC with equal closed-loop bandwidth, it has been assumed that the controlled variable of the ROC is the direct axis flux, computed on the basis of the direct axis self-inductance at the rated current. Afterwards, the direct current controller gains have been scaled according to the constant gain introduced by the direct axis self-inductance, so as to guarantee that the closed-loop bandwidth of the two controllers are equal.

Using the controllers tuned with the parameters given in Table II, for both ROC and FL, the Bode diagrams of the transfer functions of the open-loop systems, plotted in Figs. 5 and 6, are obtained. From these figures, it can be easily observed that the two systems, respectively, SynRM controlled with FL and SynRM controlled with ROC, have the same crossing pulsation and the same phase margin, as shown in Table III. Moreover, Figs. 7 and 8 show the Bode diagrams of the closed-loop transfer functions. From these figures, it is possible to see that the same closed-loop bandwidths are obtained, equal to about $B_{-3\text{db}} = 47.5$ rad/s for the direct axis flux loop and $B_{-3\text{db}} = 3.37$ rad/s for the speed loop. Figs. 5 and 6 clearly show that the controllers have been designed so as to guarantee a phase margin of 45° and a gain margin equal to infinity for both the controllers. It inherently implies the stability of the system. Moreover, the definition of the nonlinear transformation of the states and inputs in (14) and (18) guarantees that such a stability margin is guaranteed in each operating condition, independently from the magnetic saturation.

However, to obtain the transfer functions in the ROC case, the assumptions of constant parameters and constant direct axis flux amplitude should be made. In particular, for the transfer function of the flux as well as for the transfer function of the speed, the parameters obtained at rated currents are considered. This represents a limitation for the ROC as compared with the FL: In the FL, the specifics given in Table III are satisfied in all working conditions, while in the ROC, these specifics could change if the flux level is different from the rated one (condition always happening under MTPA). They are, therefore, rigorously respected in only one working condition. This fact is evident because if the motor is controlled by FLC, the closed-loop transfer function can be deduced from (15) and (23) where no physical parameters appear, while if the motor is controlled by ROC, the closed-loop transfer function contains the machine parameters that are varying with currents due to the saturation effects [e.g., the inductances in (4)–(6)].

C. Comparison Between the Proposed FL and ROC

The proposed FL overcomes ROC in terms of performance in both constant direct axis flux and variable direct axis flux working conditions. The reason that it overcomes ROC in variable direct axis flux conditions is that it can cover the nonlinearity due to the torque expression. In fact, a coupling exists between the speed and the direct axis current (direct axis flux) loops, and a related nonlinearity in the system, between the direct (x) and quadrature (y) axes in variable flux working condition due to fact that the electromagnetic torque is proportional to the product between the direct and quadrature current components. The capability of correctly decoupling the speed and the direct axis current (flux) loops in variable direct axis flux working conditions is a standard prerogative of FL, while it is not of ROC [10]. The reason that the proposed FL overcomes ROC even in constant direct axis flux conditions is that it can cover the nonlinearity due to the magnetic saturation, which is a peculiar prerogative of this specific version of FL. Thanks to this feature, the controlled system presents always the same dynamics with a controller characterized by a fixed structure, independently from the operating point (independently from the flux and load values). This is not the case of the ROC, presenting a dynamic variable with the operating conditions because of the variations of the inductances with the magnetic saturation.

IV. Test Setup

The employed test setup consists of a SynRM motor ABB 3GALO92543-BSB whose rated data are given in Table IV. Table V shows the parameters of the complete saturation model, identified with the technique proposed in [32]. The SynRM is supplied by a VSI with insulated gate bipolar transistor modules, model Semikron SMK 5O GB 123, driven by a space-vector pulsewidth modulation (SV-PWM) technique with PWM frequency set to 5 kHz. The adopted control technique has been implemented on a dSPACE card (DS1103) with a PowerPC 604e at 400 MHz and a fixed-point DSP TMS320F240. The sampling time of controller has been set to 10 kHz. The SynRM motor is mechanically coupled to a torque controlled permanent magnet synchronous motor drive working as active load. Fig. 9 shows the photograph of the SynRM drive test setup.

V. Experimental Results

The proposed FLC technique, specifically developed for SynRM drives, has been experimentally compared with the ROC. The test setup described in Section IV has been exploited for this purpose. As for the adopted version of the ROC, an ROC has been used [5]. Both the FLC and the ROC controllers have been tuned so as to present the same dynamic performance, as fully explained in Section III-A. Moreover, some tests have been made in constant flux and other in variable flux working conditions. As for the variable flux operation, the SynRM drive has been integrated with the MTPA technique as proposed in [18]. This is a very challenging working condition, in which FLC is theoretically expected to overcome ROC in terms of dynamic performance. As for the field weakening (constant power) and

Authorized licensed use limited to: University of the South Pacific. Downloaded on June 08,2022 at 06:52:22 UTC from IEEE Xplore. Restrictions apply.

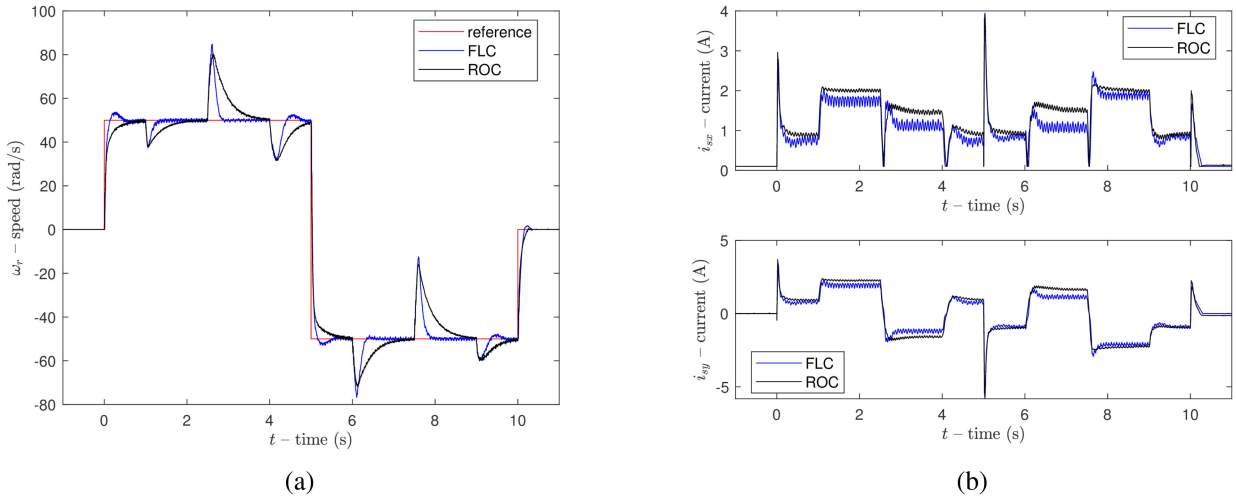

Fig. 10. (a) Reference and measured speed and (b) currents i_{sx} and i_{sy}, during a four-quadrant test with contemporary variation of flux and load.

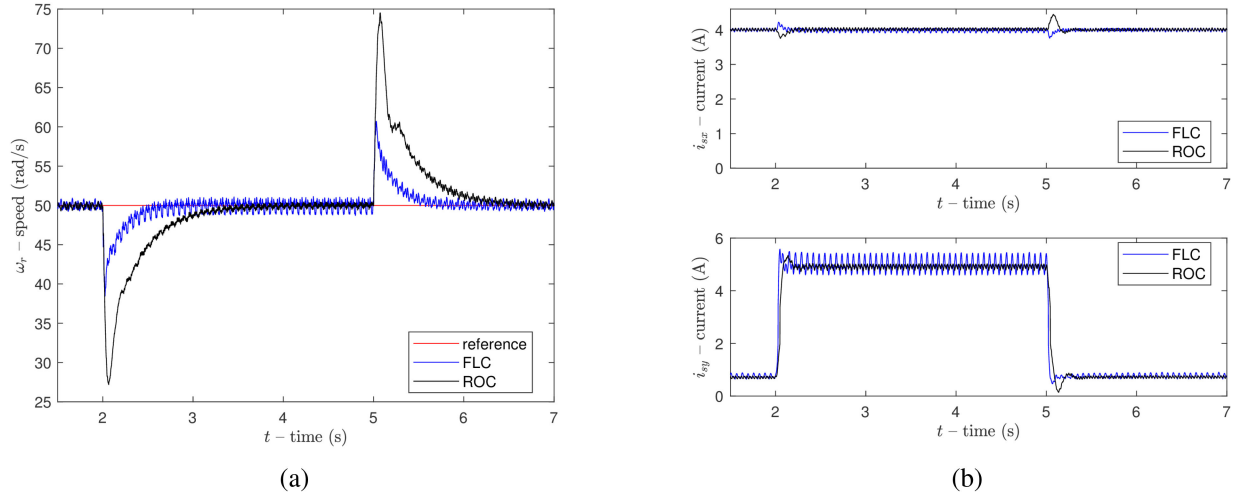

Fig. 11. (a) Reference and measured speed and (b) currents i_{sx} and i_{sy}, during a test with constant flux and speed, and load steps.

maximum torque per voltage (MPTV) (reduced power) working regions, [33] clearly highlights that field weakening and MPTV can be performed regulating the direct component of the stator current (exactly with the same logic of MTPA). Such an approach could be thus easily integrated in the proposed FLC to cover the reduced power speed range. This is, however, out of the scope of this article. Test 1 is a four-quadrant test. Such a test has been performed in variable flux working conditions. The SynRM drive, starting from zero speed, has been first given a speed step reference of 50 rad/s at no-load. Once the drive has properly tracked the reference speed, a load step torque of 2.5 N · m is applied (corresponding to 25% of the rated load), exploiting the PMSM drive as active load. Once the speed controller has governed the drive speed back to its reference, the load torque is modified with a step from 2.5 to –2.5 N · m (making the drive work in regenerative mode). Afterwards, the load is released and a speed reversal from 50 to –50 rad/s is commanded at no-load. Once the drive has tracked the reference speed of –50 rad/s, a step load torque of 2.5 N · m is first applied (making the drive work in regenerative mode) after which a load step of –2.5 N · m is applied. Fig. 10(a) shows the reference and measured speeds, obtained respectively with the proposed FLC and with the ROC. Fig. 10(b) shows the corresponding waveforms of the i_{sx} and i_{sy} stator current components. The speed waveform shows clearly that both the proposed FLC and the ROC guarantee a very fast dynamic response as well as a null steady-state tracking error. The dynamic performance achieved with the proposed FLC is, however, better than that obtained with ROC. The rise time obtained with the FLC is clearly lower, even if theoretically both FLC and ROC present the same closed-loop bandwidth. Fig. 13 shows the integral absolute error (IAE) as well as the overshoots and rise times/settling times computed on the speed loop. It confirms that the IAE presented by the FLC is always much lower than that presented by ROC, which is almost one order smaller in all cases. They clearly highlight that FLC significantly overcomes ROC in terms of dynamic performance in both transient response and load rejection capability. As for the stator current waveforms,

Authorized licensed use limited to: University of the South Pacific. Downloaded on June 08,2022 at 06:52:22 UTC from IEEE Xplore. Restrictions apply.

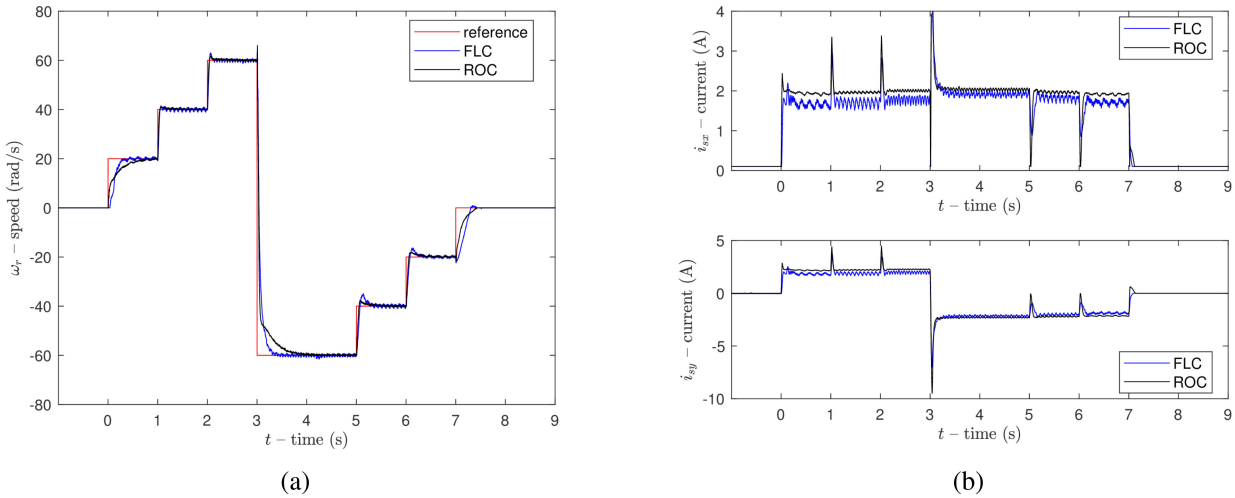

Fig. 12. (a) Reference and measured speed and (b) currents i_{sx} and i_{sy}, during a test with speed steps and MTPA conditions, at load.

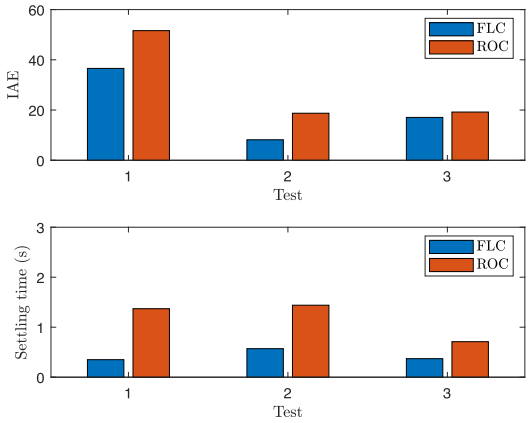

Fig. 13. Performance indexes.

i_{sy} presents a stepwise waveform with positive (negative) peaks at either each positive (negative) variation of the reference speed or positive (negative) step of load torque. Correspondingly, even i_{sx} presents the same shape, with an increase of i_{sx} at each speed step, because of the MTPA. A slightly different value of i_{sx} with the FLC and ROC can be observed, which is due to the set of nonlinear transformation present in the FLC and not present in ROC where a cascaded loop control is operated. Test 2 is a load rejection test. Such a test has been performed in constant flux working conditions. The SynRM drive is operated at a constant speed of 50 rad/s. A step load torque of 10 N · m has been first applied and then released to the SynRM drive. The test has been performed with the machine magnetized at constant level (i_{sx} = 4.5 A). Fig. 11(a) shows the reference and measured speeds obtained, respectively, with the proposed FLC and with the ROC. Fig. 11(b) shows the corresponding waveforms of the i_{sx} and i_{sy} stator current components. It can be clearly observed that, even in constant flux operation, FLC presents a far better load rejection than that presented by ROC: After the application or release of the load torque, the measured speed approaches its reference much faster in the FLC case than in the ROC one. These results are consistent with what is expected theoretically, confirmed by the IAE indexes and settling times shown in Fig. 13. Test 3 is a fast speed-transient test at light load. Such a test has been performed in variable flux working conditions. A set of speed step references including a speed reversal, of the type 0→ 20 → 40 → 60 →–60→-40→–20→0 rad/s, has been given the drive, while it is subjected to a constant load equal to 2.5 N · m, corresponding to 25% of the rated load. Fig. 12(a) shows the reference and measured speeds obtained, respectively, with the proposed FLC and with the ROC. Fig. 12(b) shows the corresponding waveforms of the i_{sx} and i_{sy} stator current components. It can be observed that both FLC and ROC present good dynamic performance in speed control. The measured speed correctly tracks its reference with a low rise time and null tracking error. Since the drive is constantly loaded with 25% of the rated torque, it can accelerate/decelerate exploiting just the difference between the maximum torque and the load one. This is the reason that FLC outperforms ROC less in this test than in the former ones, as clearly emphasized by the IAE index in Fig. 13.

Finally, the last test is related to rated load and rated speed operation under MTPA. The SynRM drive has been given a reference speed equal to the rated speed of 150 rad/s at no-load. Afterwards, at $t = 2$ s, a step torque equal to the rated load of 14 N · m has been applied, exploiting the PMSM drive as active load. Fig. 14(a) shows the reference and measured speeds during this test, while Fig. 14(b) shows the corresponding i_{sx} and i_{sy} current components. The speed curve shows that the measured speed correctly tracks its reference at no-load. As soon as the rated step torque is applied to the drive, the measured speed reduces, but the control system suddenly reacts increasing the electromagnetic torque so that in less than 1 s, the measured speed gets its reference. The dual situation happens as soon as the load rated torque is released. The current waveforms are coherent with the speed one. While the drive is running at no-load, i_{sy} is controlled at a minimum value permitting to cope the mechanical friction losses. When the rated load is applied, i_{sy} increases suddenly in order to compensate the load. According

Authorized licensed use limited to: University of the South Pacific. Downloaded on June 08,2022 at 06:52:22 UTC from IEEE Xplore. Restrictions apply.

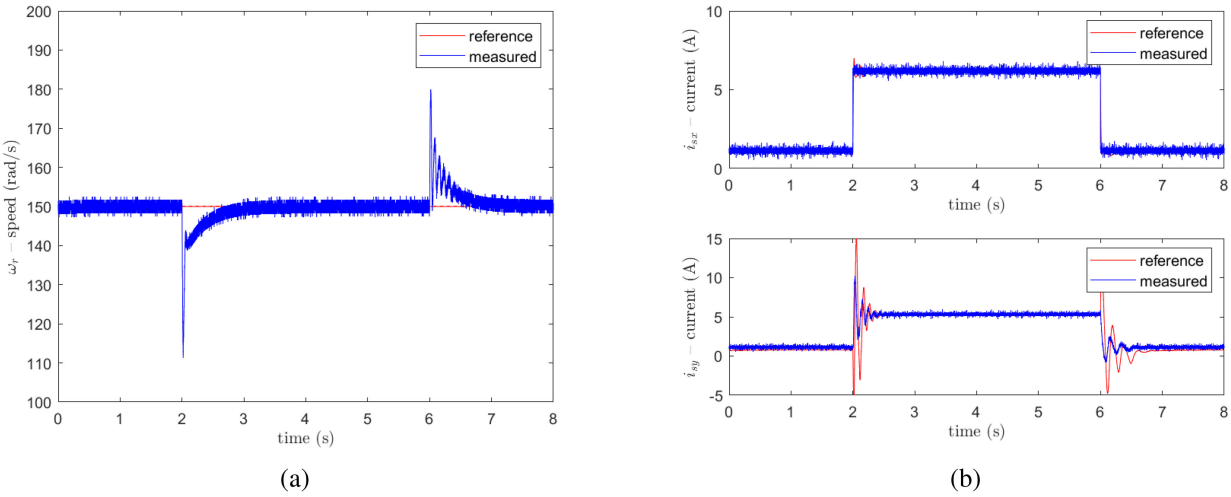

Fig. 14. (a) Reference and measured speed and (b) currents i_{sx} and i_{sy} during rated load and rated speed operation.

to the MTPA logic, i_{sx} presents almost the same shape as that of i_{sy}. All these figures witness the correct load rejection capability of the drive at rated values.

A. FLC Behavior Under Detuned Working Conditions

Input–output FL is a very powerful nonlinear control technique, theoretically guaranteeing better dynamic performance than ROC (or FOC). FLC, however, strongly relies on the following two aspects.

1) The accuracy of the model underlying the FLC; for this reason, a dynamic model accounting for the magnetic saturation including cross-saturation has been suitably defined and exploited.
2) The correctness of the model's parameters; with this regard, a specific parameter estimation technique has been developed permitting all the model parameters to be properly identified [32].

In general, the unperfect knowledge of the model's parameters causes the presence of a nonnull tracking error and a modification of the dynamic performance of the FLC controller. Such effects are quite hardly predictable in advance. In order to verify the sensitivity of the proposed FLC versus the variation of the main parameters of the SynRM model, some tests have been performed under strongly detuned working conditions. The sensitivity of the proposed FLC versus the variation of R_s, L_{sxx}, and L_{syy} has been analyzed. In particular, R_s has been varied of 100%, while L_{sxx} and L_{syy} have been varied of $\pm 50\%$. Three operating speeds have been chosen: 10 (low speed), 100 (below rated speed), and 200 rad/s (field weakening).

Fig. 15 shows the reference and measured speeds as well as the direct axis current with the FLC. With the controller properly tuned, the FLC exhibits the expected dynamic behavior, in accordance with the controller design described in Section III-A. Moreover, the steady-state tracking errors of both the speed and direct axis loops are null because the chosen linear controller has a pole in the origin of the complex plane.

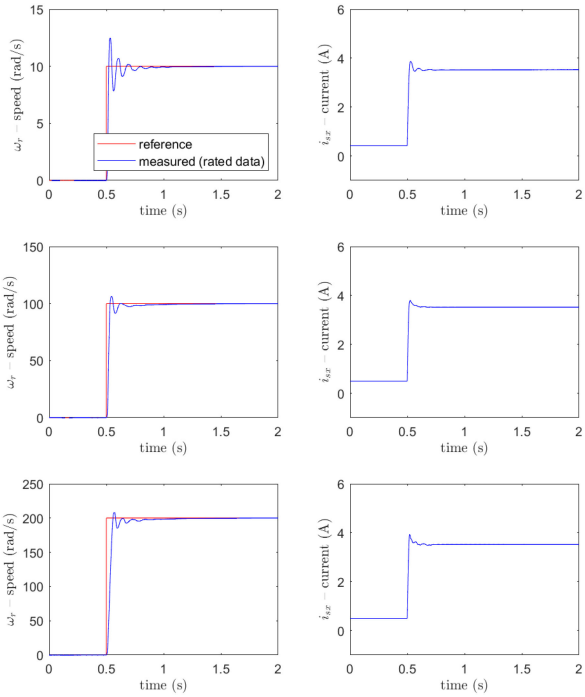

Fig. 15. Reference and measured speeds and the direct axis current with the FLC properly tuned.

Fig. 16 shows the case of $\pm 50\%$ of variation of L_{sxx}. The same test has been made at 10 (low speed), 100 (below rated speed), and 200 rad/s (field weakening). Figs. 17 and 18 show the same kinds of waveform related to the variations of L_{syy} and R_s. These figures clearly show that the effects of the detuning of L_{sxx} are almost negligible at low speed, while it is visible at medium speed and becomes critical at high speed, in particular in field weakening, as expected. The effect is more visible on the current than on the speed. As for L_{syy}, the effect of the detuning is perfectly observable even at low speed, becoming significant at increasing speeds, with critical oscillations of both the speed and current. The detuning of the stator resistance presents a dual

Authorized licensed use limited to: University of the South Pacific. Downloaded on June 08,2022 at 06:52:22 UTC from IEEE Xplore. Restrictions apply.

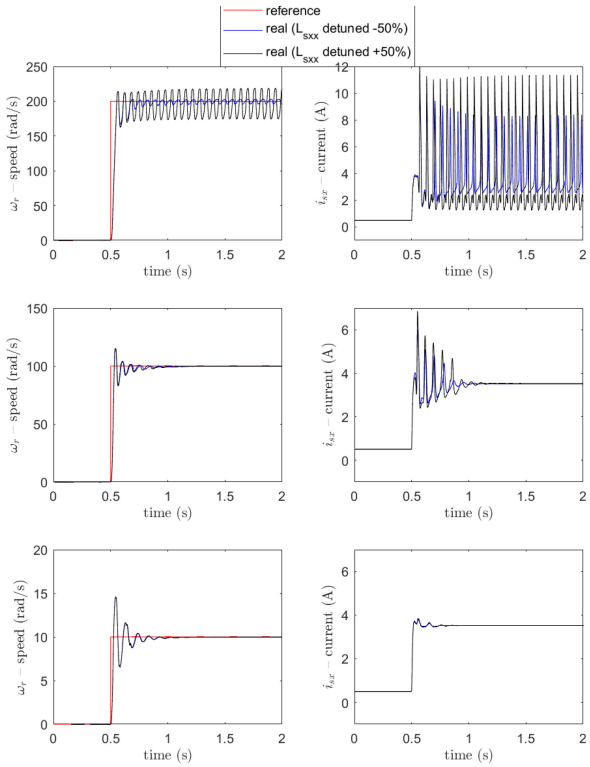

Fig. 16. Reference and measured speeds and the direct axis current with the FLC with the L_{sxx} and L'_{sxx} detuned of $\pm 50\%$.

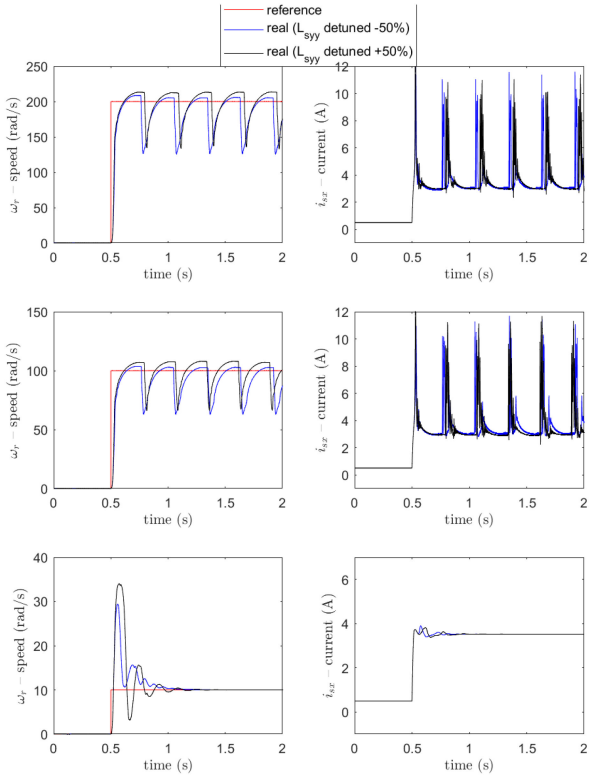

Fig. 17. Reference and measured speeds and the direct axis current with the FLC with the L_{syy} and L'_{syy} detuned of $\pm 50\%$.

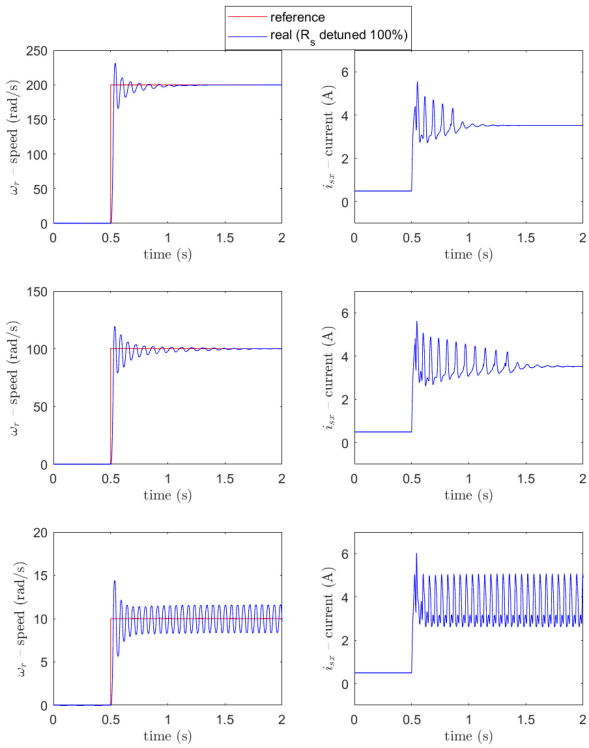

Fig. 18. Reference and measured speeds and the direct axis current with the FLC with the R_s detuned of 100%.

behavior. It is almost negligible at high speed, while it becomes significant at low speed. The above figures clearly show that the imperfect knowledge of the inductances can be very critical for the control performance and thus fully justify the integration of a suitably developed magnetic model in the proposed FLC.

It should be finally noted that the steady-state error is null, even in the presence of a strong detuning of the parameters. This is due to the chosen structure of the controller.

VI. Conclusion

This article proposes a nonlinear controller based on input–output FL for SynRMs motor drives which takes into consideration the magnetic saturation. The proposed nonlinear FL-based control technique has been developed starting from the theoretical definition of an original dynamic model of the SynRM taking into consideration both the self- and the cross-saturation effects. Such a control technique permits the dynamics of both the speed and flux loops to be maintained constant independently of the load and the saturation of the iron core in both constant flux and variable flux operating conditions. The proposed technique has been tested experimentally on a suitably developed test setup. It has been further experimentally compared with FOC in both constant and variable flux operations, exhibiting better dynamic performance in both working conditions. Finally, the limited degradation of the performance of the proposed FLC versus the variation of the main motor parameters has been further verified.

Authorized licensed use limited to: University of the South Pacific. Downloaded on June 08,2022 at 06:52:22 UTC from IEEE Xplore. Restrictions apply.

APPENDIX

$$l_{xx}=\frac{\gamma}{\sigma_1}\frac{\operatorname{sgn}(i_{sx})}{\left(\mathrm{e}^{\frac{(i_{sx}-\mu_1\operatorname{sgn}(i_{sx}))\operatorname{sgn}(i_{sx})}{2\sigma_1}}+\mathrm{e}^{-\frac{(i_{sx}-\mu_1\operatorname{sgn}(i_{sx}))\operatorname{sgn}(i_{sx})}{2\sigma_1}}\right)^2},$$

$$l_{xy}=\frac{1}{1+\mathrm{e}^{-\frac{(i_{sy}-\mu_2\operatorname{sgn}(i_{sy}))\operatorname{sgn}(i_{sy})}{\sigma_2}}},$$

$$l_{yy}=\frac{\gamma}{\sigma_2}\frac{\operatorname{sgn}(i_{sy})}{\left(\mathrm{e}^{\frac{(i_{sy}-\mu_2\operatorname{sgn}(i_{sy}))\operatorname{sgn}(i_{sy})}{2\sigma_2}}+\mathrm{e}^{-\frac{(i_{sy}-\mu_2\operatorname{sgn}(i_{sy}))\operatorname{sgn}(i_{sy})}{2\sigma_2}}\right)^2},$$

$$l_{yx}=\frac{1}{1+\mathrm{e}^{-\frac{(i_{sx}-\mu_1\operatorname{sgn}(i_{sx}))\operatorname{sgn}(i_{sx})}{\sigma_1}}},$$

$$l'_x=\frac{\mathrm{e}^{\frac{(i_{sx}-\mu_1\operatorname{sgn}(i_{sx}))\operatorname{sgn}(i_{sx})}{2\sigma_1}}-\mathrm{e}^{-\frac{(i_{sx}-\mu_1\operatorname{sgn}(i_{sx}))\operatorname{sgn}(i_{sx})}{2\sigma_1}}}{\mathrm{e}^{\frac{(i_{sx}-\mu_1\operatorname{sgn}(i_{sx}))\operatorname{sgn}(i_{sx})}{2\sigma_1}}+\mathrm{e}^{-\frac{(i_{sx}-\mu_1\operatorname{sgn}(i_{sx}))\operatorname{sgn}(i_{sx})}{2\sigma_1}}},$$

$$l'_y=\frac{\mathrm{e}^{\frac{(i_{sy}-\mu_2\operatorname{sgn}(i_{sy}))\operatorname{sgn}(i_{sy})}{2\sigma_2}}-\mathrm{e}^{-\frac{(i_{sy}-\mu_2\operatorname{sgn}(i_{sy}))\operatorname{sgn}(i_{sy})}{2\sigma_2}}}{\mathrm{e}^{\frac{(i_{sy}-\mu_2\operatorname{sgn}(i_{sy}))\operatorname{sgn}(i_{sy})}{2\sigma_2}}+\mathrm{e}^{-\frac{(i_{sy}-\mu_2\operatorname{sgn}(i_{sy}))\operatorname{sgn}(i_{sy})}{2\sigma_2}}}.$$

REFERENCES

[1] A. Accetta, M. Cirrincione, M. Pucci, and A. Sferlazza, "A nonlinear control of synchronous reluctance motors (SynRM) based on feedback linearization considering the self and cross-saturation effects," in *Proc. Energy Convers. Congr. Expo.*, 2019, pp. 1804–1809.

[2] P. Vas, *Sensorless Vector and Direct Torque Control*. Oxford, U.K.: Oxford Univ. Press, 1998.

[3] L. Xu, X. Xu, T. A. Lipo, and D. W. Novotny, "Vector control of a synchronous reluctance motor including saturation and iron loss," *IEEE Trans. Ind. Appl.*, vol. 27, no. 5, pp. 977–985, Sep./Oct. 1991.

[4] R. E. Betz, R. Lagerquist, M. Jovanovic, T. J. Miller, and R. H. Middleton, "Control of synchronous reluctance machines," *IEEE Trans. Ind. Appl.*, vol. 29, no. 6, pp. 1110–1122, Nov./Dec. 1993.

[5] A. Vagati, M. Pastorelli, and G. Franceschini, "High-performance control of synchronous reluctance motors," *IEEE Trans. Ind. Appl.*, vol. 33, no. 4, pp. 983–991, Jul./Aug. 1997.

[6] K. Uezato, T. Senjyu, and Y. Tomori, "Modeling and vector control of synchronous reluctance motors including stator iron loss," *IEEE Trans. Ind. Appl.*, vol. 30, no. 4, pp. 971–976, Jul./Aug. 1994.

[7] G. Pellegrino, R. I. Bojoi, and P. Guglielmi, "Unified direct-flux vector control for AC motor drives," *IEEE Trans. Ind. Appl.*, vol. 47, no. 5, pp. 2093–2102, Sep./Oct. 2011.

[8] H. K. Khalil, *Nonlinear Systems*, vol. 3. Englewood Cliffs, NJ, USA: Prentice-Hall, 2002.

[9] A. Isidori, *Nonlinear Control Systems*, 3rd ed. Berlin, Germany: Springer, 1995.

[10] R. Marino, P. Tomei, and C. M. Verrelli, *Induction Motor Control Design*. Berlin, Germany: Springer, 2010.

[11] R. Marino, S. Peresada, and P. Valigi, "Adaptive input-output linearizing control of induction motors," *IEEE Trans. Autom. Control*, vol. 38, no. 2, pp. 208–221, Feb. 1993.

[12] C. Lascu, S. Jafarzadeh, M. S. Fadali, and F. Blaabjerg, "Direct torque control with feedback linearization for induction motor drives," *IEEE Trans. Power Electron.*, vol. 32, no. 3, pp. 2072–2080, Mar. 2017.

[13] H. A. Zarchi, J. Soltani, A. Maleknia, and G. R. A. Markadeh, "A Lyapunov based nonlinear speed tracking controller for synchronous reluctance motor using adaptive input-output feedback linearization technique," in *Proc. Int. Conf. Ind. Technol.*, 2008, pp. 1–5.

[14] H. A. Zarchi, J. Soltani, and G. A. Markadeh, "Adaptive input-output feedback-linearization-based torque control of synchronous reluctance motor without mechanical sensor," *IEEE Trans. Ind. Electron.*, vol. 57, no. 1, pp. 375–384, Jan. 2010.

[15] H.-D. Lee, S.-J. Kang, and S.-K. Sul, "Efficiency-optimized direct torque control of synchronous reluctance motor using feedback linearization," *IEEE Trans. Ind. Electron.*, vol. 46, no. 1, pp. 192–198, Feb. 1999.

[16] M. Nabipour, H. A. Zarchi, and S. Madani, "Robust position control of synchronous reluctance motor drives using linear variable structure and adaptive input-output feedback linearization approaches," in *Proc. Iranian Conf. Elect. Eng.*, 2011, pp. 1–5.

[17] H. A. A. Awan, M. Hinkkanen, R. Bojoi, and G. Pellegrino, "Stator-flux-oriented control of synchronous motors: A systematic design procedure," *IEEE Trans. Ind. Appl.*, vol. 55, no. 5, pp. 4811–4820, Sep./Oct. 2019.

[18] A. Accetta, M. Cirrincione, M. C. Di Piazza, G. La Tona, M. Luna, and M. Pucci, "Analytical formulation of a maximum torque per ampere (MTPA) technique for SynRMs considering the magnetic saturation," *IEEE Trans. Ind. Appl.*, vol. 56, no. 4, pp. 3846–3854, Jul./Aug. 2020.

[19] A. Accetta, M. Cirrincione, M. Pucci, and A. Sferlazza, "A space-vector state dynamic model of the synchronous reluctance motor including self and cross-saturation effects and its parameters estimation," in *Proc. Energy Convers. Congr. Expo.*, 2018, pp. 4466–4472.

[20] A. Accetta, M. Cirrincione, M. Pucci, and A. Sferlazza, "A saturation model of the synchronous reluctance motor and its identification by genetic algorithms," in *Proc. Energy Convers. Congr. Expo.*, 2018, pp. 4460–4465.

[21] Z. Qu, T. Tuovinen, and M. Hinkkanen, "Inclusion of magnetic saturation in dynamic models of synchronous reluctance motors," in *Proc. Int. Conf. Elect. Mach.*, 2012, pp. 994–1000.

[22] H. De Jong, "Saturation in electrical machines," in *Proc. Int. Conf. Elect. Mach.*, vol. 80, 1980, pp. 1545–1552.

[23] K. Corzine, B. T. Kuhn, S. Sudhoff, and H. Hegner, "An improved method for incorporating magnetic saturation in the QD synchronous machine model," *IEEE Trans. Energy Convers.*, vol. 13, no. 3, pp. 270–275, Sep. 1998.

[24] C. Mademlis, "Compensation of magnetic saturation in maximum torque to current vector controlled synchronous reluctance motor drives," *IEEE Trans. Energy Convers.*, vol. 18, no. 3, pp. 379–385, Sep. 2003.

[25] T. Tuovinen, M. Hinkkanen, and J. Luomi, "Analysis and design of a position observer with resistance adaptation for synchronous reluctance motor drives," *IEEE Trans. Ind. Appl.*, vol. 49, no. 1, pp. 66–73, Jan./Feb. 2013.

[26] A. Kilthau and J. Pacas, "Appropriate models for the control of the synchronous reluctance machine," in *Proc. Conf. Rec. IEEE Ind. Appl. Conf.*, vol. 4, 2002, pp. 2289–2295.

[27] S. Yamamoto, K. Tomishige, and T. Ara, "A method to calculate transient characteristics of synchronous reluctance motors considering iron loss and cross-magnetic saturation," in *Proc. Conf. Rec. IEEE Ind. Appl. Conf.*, vol. 3, 2005, pp. 1754–1761.

[28] E. Armando, P. Guglielmi, G. Pellegrino, M. Pastorelli, and A. Vagati, "Accurate modeling and performance analysis of IPM-PMASR motors," *IEEE Trans. Ind. Appl.*, vol. 45, no. 1, pp. 123–130, Jan./Feb. 2009.

[29] A. Vagati, M. Pastorelli, F. Scapino, and G. Franceschini, "Impact of cross saturation in synchronous reluctance motors of the transverse-laminated type," *IEEE Trans. Ind. Appl.*, vol. 36, no. 4, pp. 1039–1046, Jul./Aug. 2000.

[30] N. Bedetti, S. Calligaro, and R. Petrella, "Stand-still self-identification of flux characteristics for synchronous reluctance machines using novel saturation approximating function and multiple linear regression," *IEEE Trans. Ind. Appl.*, vol. 52, no. 4, pp. 3083–3092, Jul./Aug. 2016.

[31] H. Mahmoud, G. Bacco, M. Degano, N. Bianchi, and C. Gerada, "Synchronous reluctance motor iron losses: Considering machine nonlinearity at MTPA, FW, and MTPV operating conditions," *IEEE Trans. Energy Convers.*, vol. 33, no. 3, pp. 1402–1410, Sep. 2018.

[32] A. Accetta, M. Cirrincione, M. Pucci, and A. Sferlazza, "Space-vector state dynamic model of SynRM considering self-and cross-saturation and related parameter identification," *IET Electric Power Appl.*, vol. 14, no. 14, pp. 2798–2808, 2021.

[33] L. Sepulchre, M. Fadel, M. Pietrzak-David, and G. Porte, "MTPV flux-weakening strategy for PMSM high speed drive," *IEEE Trans. Ind. Appl.*, vol. 54, no. 6, pp. 6081–6089, Dec. 2018.

Authorized licensed use limited to: University of the South Pacific. Downloaded on June 08,2022 at 06:52:22 UTC from IEEE Xplore. Restrictions apply.

Angelo Accetta (Member, IEEE) received the master's degree in electrical engineering in 2008 from the University of Palermo, Palermo, Italy, where he received the Ph.D. degree in electrical engineering, in collaboration with the Institute for Studies on Intelligent Systems for Automation (ISSIA) - National Research Council (CNR), Palermo, Italy, in 2011.

From 2013 to 2018, he was a Junior Researcher with the Section of Palermo, ISSIA-CNR, working to new energy management strategies for distributed generation systems and to the implementation of new sensorless control strategies for permanent magnet synchronous electric motors (PMSM) and for induction motors both rotating (RIM) and linear (LIM). He is currently a Junior Researcher with the Institute of Marine Engineering (INM), CNR. His research interests include sensorless control systems for electric drives with induction, i.e., rotating and linear, motors, with particular attention to their applications for electric generation systems and electric propulsion.

Maurizio Cirrincione (Senior Member, IEEE) received the Laurea degree in electrical engineering from the Polytechnic University of Turin, Turin, Italy, in 1991 and the Ph.D. degree in electrical engineering from the University of Palermo, Palermo, Italy, in 1996.

From 1996 to 2005, he was a Researcher with the Section of Palermo, Institute for Studies on Intelligent Systems for Automation (ISSIA) - National Research Council (CNR), Palermo, Italy. In 2005, he joined the University of Technology of Belfort-Montbeliard, Belfort, France, as a Full Professor. He is currently the Head of the "School of Engineering and Physics," University of the South Pacific, Suva, Fiji. His current research interests include neural networks for modeling and control, system identification, intelligent control, power electronics, renewable energy systems, and electrical machines and drives.

Dr. Cirrincione was awarded the 1997 "E.R.Caianiello" prize for the best Italian Ph.D. thesis on neural networks.

Marcello Pucci (Senior Member, IEEE) received the Laurea and Ph.D. degrees in electrical engineering from the University of Palermo, Palermo, Italy, in 1997 and 2002, respectively.

In 2000, he was a Host Student with the Institute of Automatic Control, Technical University of Braunschweig, Braunschweig, Germany, working in the field of control of ac machines, with a grant from the German Academic Exchange Service. From 2001 to 2018, he was with the Institute of Intelligent Systems for Automation, Section of Palermo, National Research Council (CNR), Palermo, Italy. He is currently a Senior Researcher with the Institute of Marine Engineering (INM), CNR. His current research interests include electrical machines; control, diagnosis, and identification techniques of electrical drives, and intelligent control and power converters.

Dr. Pucci serves as an Associate Editor for the IEEE TRANSACTIONS ON INDUSTRIAL ELECTRONICS and IEEE TRANSACTIONS ON INDUSTRY APPLICATIONS. He is a Member of the Editorial Board of the *Journal of Electrical Systems*.

Antonino Sferlazza (Member, IEEE) was born in Palermo, Italy, in 1987. He received the master's degree in automation engineering and the Ph.D. degree in mathematics and automation from the University of Palermo, Palermo, Italy, in 2011 and 2015, respectively.

In 2013, he was a Visiting Ph.D. Student with the University of California at Santa Barbara, Santa Barbara, CA, USA, in the field of modeling and analysis of stochastic hybrid systems. From 2016 to 2017, he was with the University of Palermo as Junior Researcher. From 2017 to 2018, he was a Researcher with LAAS CNRS, Toulouse, France, working in the field of control of power converter. He is currently a Researcher in systems and control engineering with the University of Palermo. His research interests include the development of feedback control algorithms for nonlinear dynamical systems, optimization techniques, estimation of stochastic dynamical systems, and applications of control of electrical drives, power converters, and mechanical systems.

Authorized licensed use limited to: University of the South Pacific. Downloaded on June 08,2022 at 06:52:22 UTC from IEEE Xplore. Restrictions apply.